Article

Keratinocyte-specific angiotensin II receptor-associated protein deficiency exacerbates angiotensin II-dependent hypertension via activation of the skin renin-angiotensin system

Shinya Taguchi[1], Kengo Azushima [1] ✉, Kento Kitada[2], Norihiko Morisawa[3,4], Satoshi Kidoguchi [4], Ryutaro Morita[1], Kazuya Nakagawa [5], Atsushi Ishibe[5], Itaru Endo[5], Keisuke Kazama [6], Yasushi Rino[6], Aya Saito[6], Sho Kinguchi[1], Ryu Kobayashi[1], Taiji Matsusaka [7], Akio Yamashita[8], Hiromichi Wakui[1] ✉, Akira Nishiyama [2] & Kouichi Tamura [1,9]

The skin has recently been highlighted as a new player regulating blood pressure (BP). Here we show the role of skin renin-angiotensin system (RAS) in hypertension. In human subjects, skin expression of angiotensin II (Ang II) type 1 receptor (AT1R)-associated protein (ATRAP), which inhibits pathological AT1R signaling, is inversely correlated with systolic BP. Keratinocyte-specific ATRAP knockout male mice (KO) exhibit exacerbated Ang II-induced hypertension and skin-specific increases in angiotensinogen and Ang II levels. In keratinocyte-specific ATRAP and AT1R knockout male mice, Ang II-induced skin angiotensinogen excess and exaggerated hypertension seen in KO are eliminated. Although body fluid volume is comparable between the genotypes, the urine volume per water intake in Ang II-infused KO is increased, suggesting decreased extra-renal water loss, which is supported by decreased skin blood flow and transepidermal water loss in KO. Body temperature elevation-induced skin vasodilation eliminates these differences, including exaggerated hypertension, indicating the contribution of skin RAS-mediated vasoconstriction to BP elevation. Skin RAS may become a potential strategy for therapeutic interventions in hypertension.

Hypertension is the largest modifiable factor in the development of cardiovascular disease (CVD)[1], and the number of people with hypertension worldwide has doubled from 650 million to 1.28 billion over the past 30 years[2]. Furthermore, approximately 50% of patients with hypertension fail to reach the target blood pressure (BP), although various antihypertensive drugs have been intensively developed[3].

Clearly, there is an urgent need for further elucidation of the pathogenesis of hypertension and the development of alternative therapeutic targets.

Recently, accumulating evidence has indicated associations between skin and BP[4–6], and on the basis of this, two concepts have been used to explain the underlying physiological mechanisms

A full list of affiliations appears at the end of the paper. ✉e-mail: azushima@yokohama-cu.ac.jp; hiro1234@yokohama-cu.ac.jp

involved in the skin-mediated regulation of BP: "skin sodium accumulation" and "skin vasoconstriction". Magnetic resonance imaging of sodium (Na-MRI) has revealed that increased accumulation of skin sodium is associated with BP elevation in humans and rodents[7–9]. In addition, in animal models of psoriasis and renal injury, BP is elevated by skin vasoconstriction as a consequence of a compensatory mechanism against water loss from skin and kidneys to suppress transepidermal water loss (TEWL)[10–12]. However, the molecular mechanisms underlying these concepts are still largely unknown. Interestingly, similar to other tissues, the skin expresses most of the renin-angiotensin system (RAS) components, including angiotensinogen, renin, angiotensin-converting enzyme (ACE), angiotensin II (Ang II), and Ang II type 1 receptor (AT1R), which have been reported to play a physiological role in wound healing and skin fibrosis[13,14]. However, there have been no reports on the physiological or pathophysiological roles of the skin RAS in BP.

The RAS plays a central role in the regulation of BP and body fluid homeostasis, but the chronic activation of this system contributes to detrimental effects that lead to hypertension[15]. Among the RAS components, the Ang II-AT1R axis has been established as a critical factor regulating various physiological and pathophysiological signal transductions of the RAS, which link to vasoconstriction, sodium/water retention, inflammation, and fibrosis[16,17]. AT1R is locally expressed in various tissues, including the kidneys, heart, vascular smooth muscle, endothelium, and brain, and is classically considered to regulate BP and sodium/fluid homeostasis by regulating their functions[16]. As one of the RAS receptor-associated proteins, AT1R-associated protein (ATRAP) has been reported to directly bind to the carboxyl-terminal domain of AT1R to promote the constitutive internalization of AT1R from the cell surface into the cytoplasm, resulting in suppression of AT1R signaling pathways[18,19]. We reported that enhanced tissue ATRAP expression suppresses the activation of tissue AT1R signaling[20–25], whereas decreased tissue ATRAP expression accelerates the activation of this signal transduction[26–28]. Therefore, modulating tissue ATRAP expression is a useful strategy to regulate the activity of tissue-specific AT1R signaling.

In this study, we investigated the pathophysiological role of skin RAS activity in the development of hypertension using human skin samples and keratinocyte-specific genetically modified mice. Intriguingly, mRNA expression of ATRAP, but not AT1R, in the skin was significantly and negatively correlated with BP levels in human participants, and keratinocyte-specific ATRAP-deficient mice exhibited exacerbated Ang II-induced hypertension via increased skin vasoconstriction, all of which were eliminated by keratinocyte-specific AT1R deficiency or AT1R blocker (ARB) treatment. Our results indicate that skin RAS activity contributes to BP regulation and has potential as a target for the treatment of hypertension.

Results

Skin mRNA expression of ATRAP, but not AT1R, is associated with BP levels in humans

To explore the clinical association between skin RAS activity and BP, we investigated correlations between mRNA expression of *Agtr1* (gene name for AT1R) and *Agtrap* (gene name for ATRAP) in the skin and BP levels in 58 patients who underwent laparoscopic rectal cancer surgery with colostomy. The clinical characteristics of the patients are shown in Table 1. There was no significant correlation between skin *Agtr1* mRNA expression and systolic BP levels. By contrast, *Agtrap* mRNA expression in the skin was significantly and negatively correlated with systolic BP levels (Fig. 1a). Additional analyses of the human cohort without antihypertensive agents ($n = 33$) showed similar trends (Fig. 1b). There were no significant correlations between diastolic BP levels and skin mRNA expression of *Agtr1* or *Agtrap* (Supplementary Fig. 1a, b).

Keratinocyte-specific ATRAP deletion exacerbates Ang II-induced hypertension

The results of the human experiments prompted us to investigate whether skin-specific ATRAP deficiency could exacerbate arterial hypertension. Therefore, we used the Cre-loxP system to generate mice lacking ATRAP specifically in keratinocytes (K14^Cre;*Agtrap*^fl/fl, KO mice). Real-time quantitative reverse transcription PCR (qRT-PCR) analysis showed that, compared with that in littermate control mice without Cre (*Agtrap*^fl/fl, Ctrl mice), mRNA expression of *Agtrap* in KO mice was < 1% in the epidermis (which is mainly composed of keratinocytes), but was similar in the dermis, heart, kidneys, liver, and muscle (Supplementary Fig. 2a). ATRAP deletion in the keratinocytes of KO mice did not affect the appearance or histological findings of the skin, suggesting that they had normal development of the skin architecture (Supplementary Fig. 2b, c). Next, we examined the effects of keratinocyte-specific ATRAP deletion on BP using the Ang II-induced hypertension model (Fig. 2a). Noninvasive BP measurements using the tail-cuff method showed that, while there was no difference in BP between vehicle-treated Ctrl and KO mice, the Ang II-induced BP elevation was significantly higher in KO mice (Fig. 2b). Heart rate was comparable between the genotypes, with and without Ang II administration (Supplementary Fig. 3a). These results were further validated by the radiotelemetry method, a system for remotely monitoring BP in awake, unrestrained mice. Similar to the results using the tail-cuff method, BP levels at baseline were comparable between the genotypes (Fig. 2c). However, Ang II-induced increases in systolic, diastolic, and mean BPs were significantly exaggerated over 24 hours in KO mice compared with those in Ctrl mice (Fig. 2c). Consistent with the BP results, the heart weight/body weight ratio was significantly higher in Ang II-infused KO mice than in Ang II-infused Ctrl mice, concomitant with increased gene expression of *Nppb* and *Acta1*, markers of cardiac hypertrophy (Fig. 2d, e). Heart rate and motor activity were
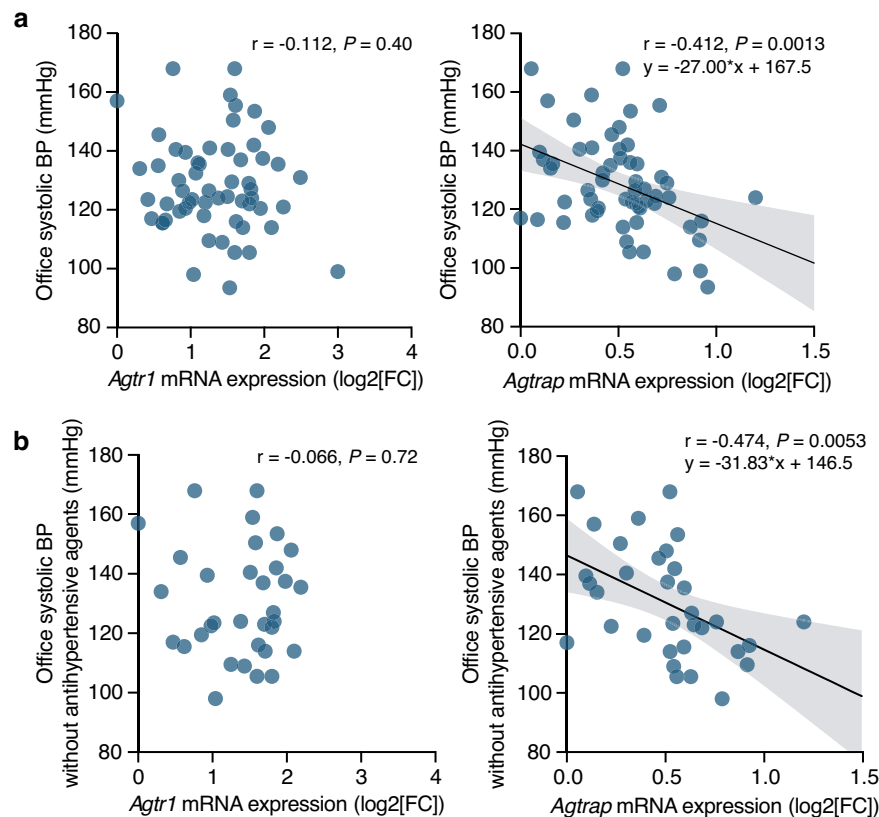
Table 1 | Baseline characteristics of the patients

Characteristics	
No. of patients	58
Age, yr	67.1 ± 12.0
Sex, n (%)	
Male	34 (58.6)
Female	24 (41.4)
Body mass index, kg/m²	24.1 ± 3.1
Hemoglobin A1c, %	5.9 ± 0.6
Estimated glomerular filtration rate, mL/min/1.73 m²	72.4 ± 15.5
Past medical history, n (%)	
Hypertension	26 (44.8)
Type 2 diabetes	12 (20.7)
Dyslipidemia	15 (25.9)
Cardiovascular disease	2 (3.4)
Office blood pressure, mmHg	
Systolic	128.5 ± 16.3
Diastolic	79.0 ± 10.4
Heart rate, beats/min	72.4 ± 9.0
Taking antihypertensive medication, n (%)	25 (43.1)
Type of antihypertensive medication, n (%)	
Renin-angiotensin system blockers	14 (24.1)
Calcium channel blockers	24 (41.3)
Diuretics	2 (3.4)
β-blockers	5 (8.6)
Aldosterone antagonists	1 (1.7)

Data expressed as means ± standard deviation, or number of patients (%).

Fig. 1 | Expression of ATRAP in human skin negatively correlates with office systolic blood pressure (BP). Linear regression models of *Agtr1* and *Agtrap* mRNA expression levels in skin and office systolic BP in human patients, including all patients ($n = 58$) (**a**) and those not taking antihypertensive agents ($n = 33$) (**b**). *Agtr1* and *Agtrap* mRNA expression levels were log-transformed, and normality was confirmed by the Shapiro-Wilk test. Two-sided linear regression analysis was performed. The line and shaded area represent the fitted regression line and the 95% confidence interval. Source data are provided as a Source Data file.

comparable between the genotypes, with and without Ang II administration (Supplementary Fig. 3b, c).

Keratinocyte-specific ATRAP deletion accelerates the activation of the skin tissue RAS in Ang II-infused mice

To investigate the effects of the keratinocyte-specific ATRAP deletion on skin tissue RAS activity, we evaluated the expression of RAS components in the skin. The expression levels of the angiotensinogen (*Agt*) and AT1R (*Agtr1a*) genes were significantly higher in Ang II-infused KO mice compared with those in Ang II-infused Ctrl mice, whereas the expression levels of the Ang II-converting enzyme (*Ace*) and renin (*Ren1*) genes were comparable between the two genotypes, with and without Ang II administration (Fig. 3a). In addition, the protein levels of angiotensinogen were significantly higher in Ang II-infused KO mice than in Ang II-infused Ctrl mice (Fig. 3b). Consistent with the results of angiotensinogen, Ang II levels in the skin were also significantly higher in Ang II-infused KO mice than in Ang II-infused Ctrl mice, whereas plasma Ang II levels were comparable between the genotypes with Ang II administration (Fig. 3c). Furthermore, in the kidneys, heart, and liver, there were no differences in the expression levels of *Agt* and *Agtr1a* between the genotypes, with and without Ang II administration, suggesting skin-specific tissue RAS activation (Supplementary Fig. 4a–c). Immunohistochemical analysis was performed to explore the localization of increased angiotensinogen expression in the skin. Angiotensinogen was predominantly stained in keratinocytes, which had the highest staining intensity in Ang II-infused KO mice (Fig. 3d). These results were confirmed western blotting analysis of epidermis samples. As expected, angiotensinogen protein levels in the epidermis were significantly increased in Ang II-infused KO mice compared with those in Ang II-infused Ctrl mice (Fig. 3e). These results indicate that

keratinocytes were the main site of angiotensinogen excess in the skin of Ang II-infused mice lacking ATRAP specifically in keratinocytes. To investigate whether changes in inflammation and/or the skin barrier and development might also affect the development of Ang II-induced hypertension in KO mice, we estimated the mRNA expressions of genes related to inflammation and the skin barrier, as well as morphological changes in the skin. mRNA expressions of *Tnf*, *Il1b*, *Il6*, and *Flg* (encoding Filaggrin) and *Tjp1* (encoding Tight junction protein ZO-1) in the skin were comparable between the genotypes with or without Ang II treatment (Supplementary Fig. 5a, b). Furthermore, under Ang II treatment, the appearance or histological findings of the skin were also comparable between the genotypes (Supplementary Fig. 5c).

Exacerbated Ang II-induced hypertension and skin tissue RAS activation in mice lacking ATRAP in keratinocytes are restored by AT1R blockade

To determine whether skin tissue RAS activation and the exacerbation of Ang II-induced hypertension in KO mice was associated with over-activated AT1R signaling, we generated keratinocyte-specific ATRAP/AT1R double-knockout mice (K14^Cre;*Agtrap*^fl/fl;*Agtr1a*^fl/fl, DKO mice). qRT-PCR analysis showed that, compared with littermate control mice without Cre (*Agtrap*^fl/fl;*Agtr1a*^fl/fl, Ctrl mice), *Agtrap* and *Agtr1a* mRNA expressions in DKO mice were < 1% in the epidermis, but similar in the dermis, heart, kidneys, liver, and muscle (Supplementary Fig. 6a, b). Furthermore, histological findings and the appearance in the skin were normal (Supplementary Fig. 6c, d). As shown in Fig. 4, the exacerbated Ang II-induced hypertension and skin angiotensinogen excess seen in KO mice were eliminated in DKO mice. Furthermore, in KO mice, ARB administration also eliminated the genotypic differences in Ang II-induced BP elevation and gene expression levels of *Agt* and *Agtr1a* in
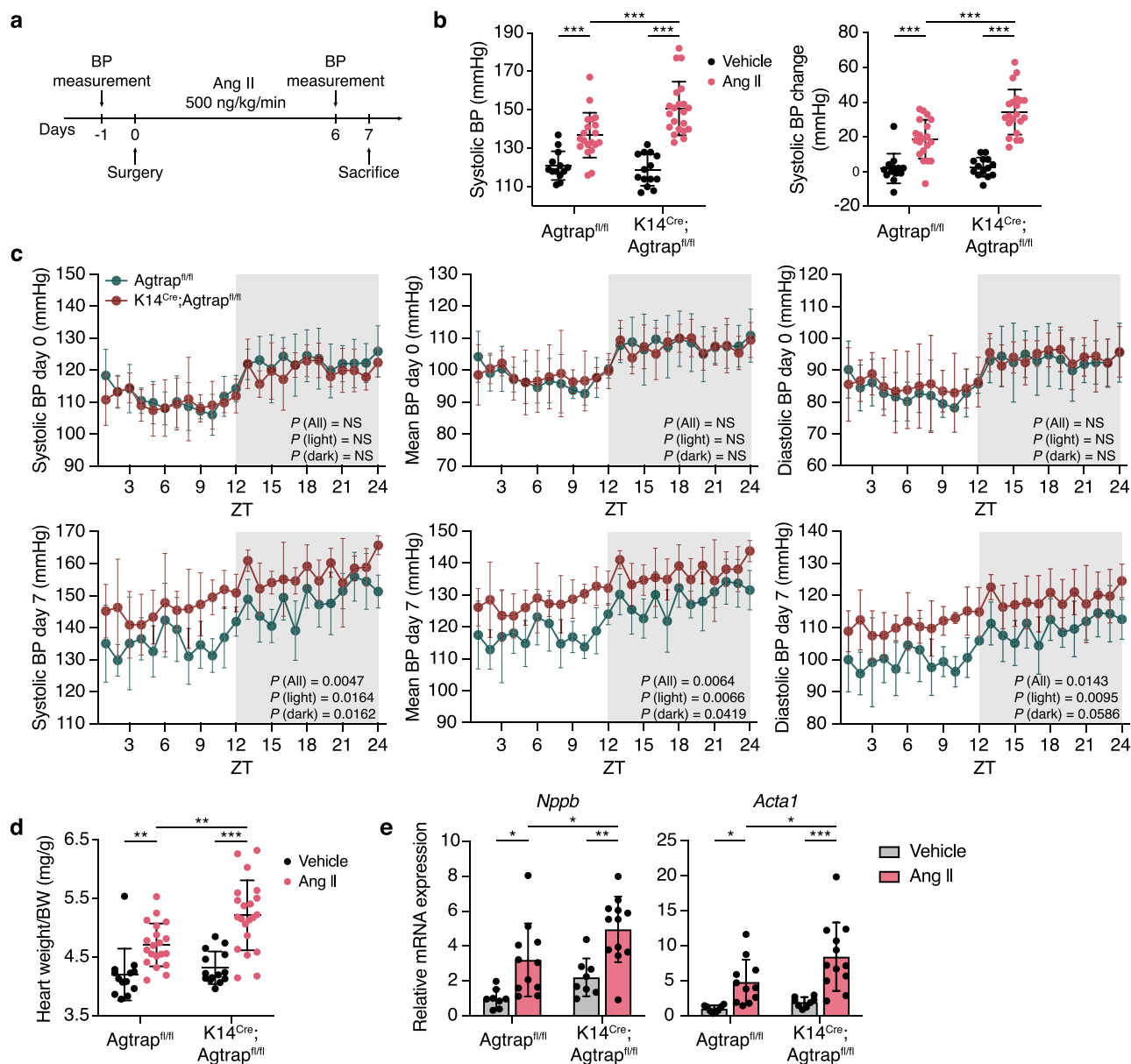
Fig. 2 | Keratinocyte-specific ATRAP deletion exacerbates angiotensin II-induced hypertension in mice. a Experimental design. **b** Systolic blood pressure (BP) and changes in BP levels assessed via the tail-cuff method in control (Ctrl) and keratinocyte-specific ATRAP knockout (KO) mice treated with vehicle or angiotensin II (Ang II); $n = 13$ (Ctrl + Vehicle), 20 (Ctrl + Ang II), 14 (KO + Vehicle), and 21 (KO + Ang II). Systolic BP: $P = 0.004$ (Ctrl + Vehicle vs. Ctrl + Ang II), $P < 0.0001$ (KO + Vehicle vs. KO + Ang II), $P = 0.004$ (Ctrl + Ang II vs. KO + Ang II). Systolic BP change: $P < 0.0001$ (Ctrl + Vehicle vs. Ctrl + Ang II), $P < 0.0001$ (KO + Vehicle vs. KO + Ang II), $P < 0.0001$ (Ctrl + Ang II vs. KO + Ang II). **c** Evaluation of systolic, mean, and diastolic BP levels using the radiotelemetry method in Ctrl and KO mice at baseline and 7 days after Ang II administration; $n = 5$. The shaded area represents the dark phase (zeitgeber time (ZT) 12–24) for mice. **d** Ratio of heart weight to body weight in Ctrl and KO mice treated with vehicle or Ang II; $n = 13$ (Ctrl+Vehicle), 20

(Ctrl + Ang II), 14 (KO + Vehicle), and 21 (KO + Ang II). $P = 0.005$ (Ctrl + Vehicle vs. Ctrl + Ang II), $P < 0.0001$ (KO + Vehicle vs. KO + Ang II), $P = 0.0013$ (Ctrl + Ang II vs. KO + Ang II). **e** *Nppb* and *Acta1* mRNA expression levels in the heart of Ctrl and KO mice treated with vehicle or Ang II; $n = 8$ (Ctrl + Vehicle), 11 (Ctrl + Ang II), 8 (KO + Vehicle), and 12 (KO + Ang II). *Nppb*: $P = 0.0122$ (Ctrl + Vehicle vs. Ctrl + Ang II), $P = 0.0015$ (KO + Vehicle vs. KO + Ang II), $P = 0.0289$ (Ctrl + Ang II vs. KO + Ang II). *Acta1*: $P = 0.0155$ (Ctrl + Vehicle vs. Ctrl + Ang II), $P = 0.0001$ (KO + Vehicle vs. KO + Ang II), $P = 0.0117$ (Ctrl + Ang II vs. KO + Ang II). Data were analyzed by two-way factorial analysis of variance (ANOVA) followed by Bonferroni's post-hoc test (**b**, **d**, and **e**), or two-way repeated measures ANOVA with Bonferroni's post-hoc test (**c**), and are expressed as means ± standard deviation. *$P < 0.05$, **$P < 0.01$, and ***$P < 0.001$. Source data are provided as a Source Data file.

the skin (Supplementary Fig. 7a, b). These findings indicate that whole skin angiotensinogen excess in Ang II-infused KO mice was mainly mediated by the Ang II-AT1R axis in keratinocytes. To more precisely estimate the effects of keratinocyte ATRAP and AT1R on BP, we also simultaneously performed an Ang II administration experiment using KO and DKO mice and their respective littermate controls, in which an exaggerated BP elevation in Ang II-infused KO mice was consistently observed across all experimental groups (Supplementary Fig. 8).

Keratinocyte-specific ATRAP deletion does not affect plasma volume, kidney function, tissue sodium accumulation, or kidney sodium handling, but does reduce TEWL in Ang II-infused mice

To investigate pathophysiological mechanisms for the exacerbation of Ang II-induced hypertension in KO mice, we evaluated plasma volume, kidney function, tissue sodium accumulation, and kidney sodium handling. There was no difference in plasma volume between the genotypes under Ang II administration (Supplementary Fig. 9a).
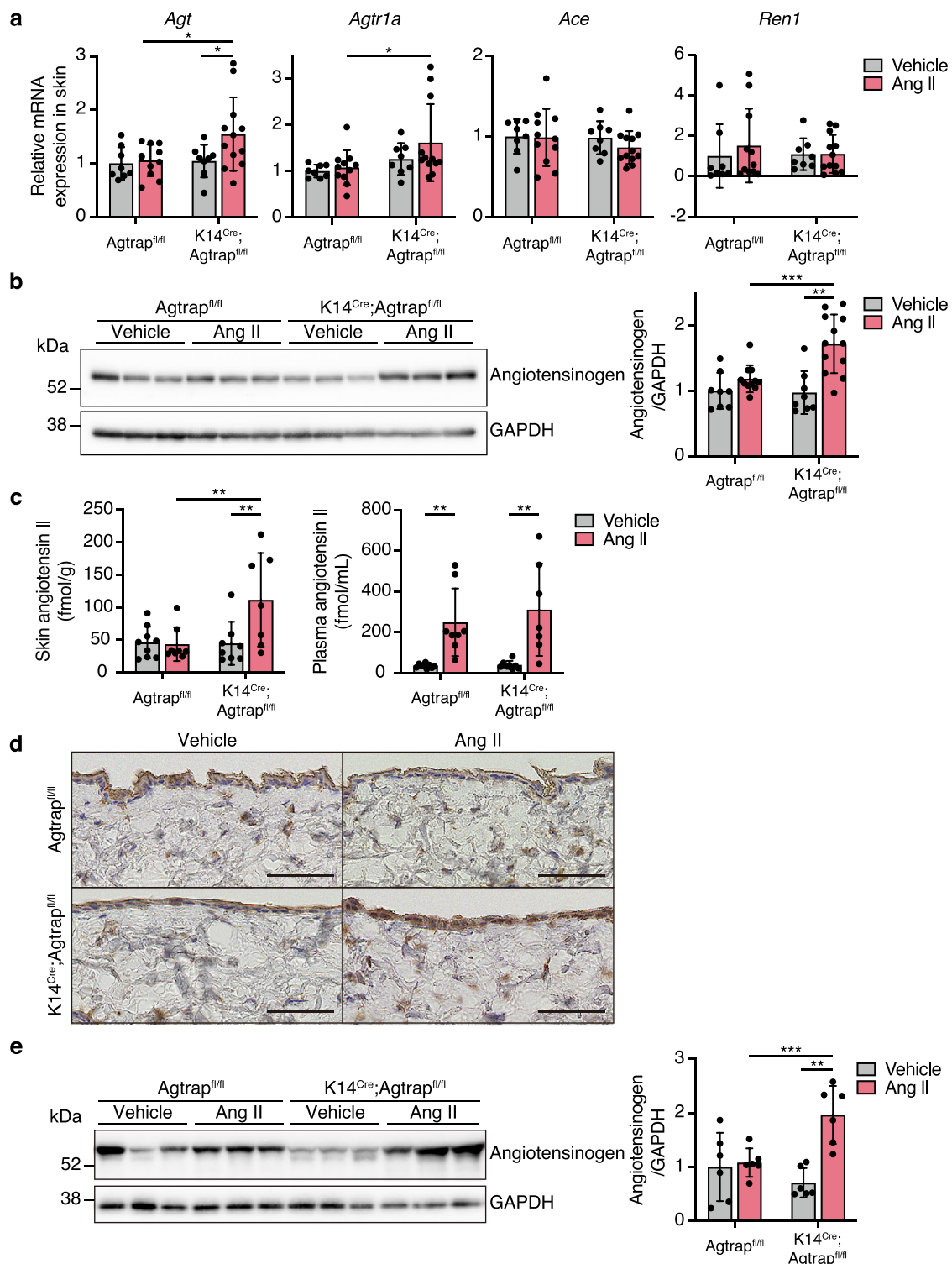
Fig. 3 | Keratinocyte-specific ATRAP deletion accelerates skin tissue RAS activation in angiotensin II-infused mice. a Expression levels of *Agt*, *Agtr1a*, *Ace*, and *Ren1* mRNA in the skin of control (Ctrl) and keratinocyte-specific ATRAP knockout (KO) mice treated with vehicle or angiotensin II (Ang II); $n = 8$ (Ctrl + Vehicle), 11 (Ctrl + Ang II), 8 (KO + Vehicle), and 12 (KO + Ang II). *Agt*: $P = 0.0424$ (KO + Vehicle vs. KO + Ang II), $P = 0.0295$ (Ctrl + Ang II vs. KO + Ang II). *Agtr1a*: $P = 0.0419$ (Ctrl + Ang II vs. KO + Ang II). **b** Immunoblot analysis of angiotensinogen protein in the skin of Ctrl and KO mice treated with vehicle or Ang II; $n = 8$ (Ctrl + Vehicle), 11 (Ctrl + Ang II), 8 (KO + Vehicle), and 12 (KO + Ang II). $P < 0.0001$ (KO + Vehicle vs. KO + Ang II), $P = 0.0011$ (Ctrl + Ang II vs. KO + Ang II). **c** Skin and plasma Ang II levels of Ctrl and KO mice treated with vehicle or Ang II; $n = 9$ (Ctrl + Vehicle), 8 (Ctrl + Ang II), 8 (KO + Vehicle), and 7 (KO + Ang II). Skin: $P = 0.0083$ (KO + Vehicle vs. KO + Ang II), $P = 0.0072$ (Ctrl + Ang II vs. KO + Ang II). Plasma: $P = 0.0056$ (Ctrl + Vehicle vs. Ctrl + Ang II), $P = 0.0011$ (KO + Vehicle vs. KO + Ang II). **d** Representative images of angiotensinogen immunostaining in the skin of Ctrl and KO mice treated with vehicle or Ang II (scale bar 50 μm). $n = 7$ (Ctrl+Vehicle), 8 (Ctrl + Ang II), 7 (KO + Vehicle), and 8 (KO + Ang II). **e** Immunoblot analysis of angiotensinogen protein in the epidermis of Ctrl and KO mice treated with vehicle or Ang II; $n = 6$. $P = 0.0002$ (KO + Vehicle vs. KO + Ang II), $P = 0.0063$ (Ctrl + Ang II vs. KO + Ang II). Data were analyzed by two-way factorial analysis of variance followed by Bonferroni's post-hoc test (**a**–**e**), and are expressed as means ± standard deviation; *$P < 0.05$, **$P < 0.01$, and ***$P < 0.001$. Source data are provided as a Source Data file.
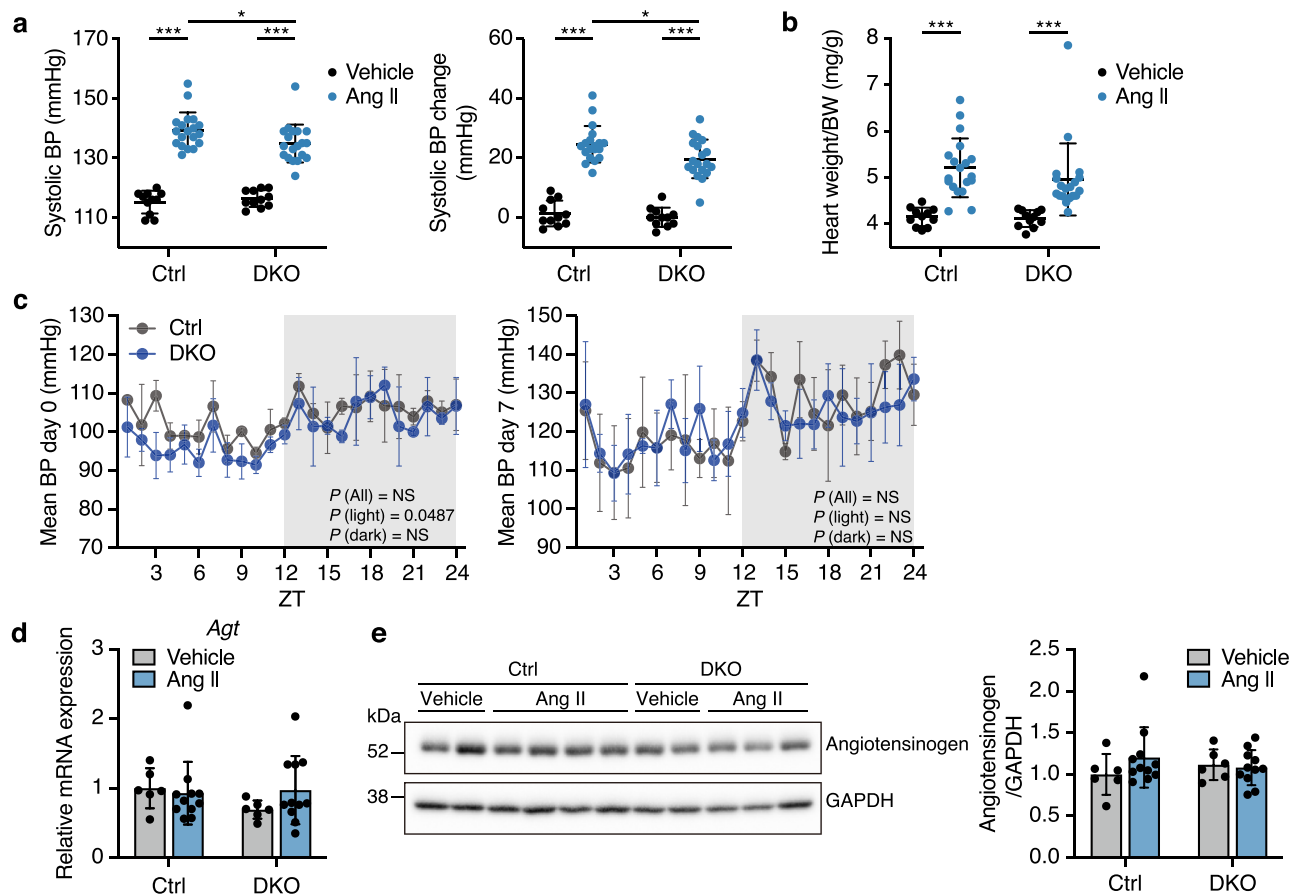
Fig. 4 | Keratinocyte-specific AT1R deletion mitigates exacerbated angiotensin II-induced hypertension and skin tissue RAS activation in keratinocyte-specific ATRAP knockout mice. a Systolic blood pressure (BP) and changes in BP levels assessed via the tail-cuff method in control (Ctrl) and keratinocyte-specific ATRAP/AT1R double knockout (DKO) mice treated with vehicle or angiotensin II (Ang II); $n = 11$ (Ctrl + Vehicle), 19 (Ctrl + Ang II), 11 (DKO + Vehicle), and 19 (DKO + Ang II). Systolic BP: $P = 0.004$ (Ctrl + Vehicle vs. Ctrl + Ang II), $P < 0.0001$ (DKO + Vehicle vs. DKO + Ang II), $P = 0.0257$ (Ctrl + Ang II vs. DKO + Ang II). Systolic BP change: $P < 0.0001$ (Ctrl + Vehicle vs. Ctrl + Ang II), $P < 0.0001$ (DKO + Vehicle vs. DKO + Ang II), $P = 0.0162$ (Ctrl + Ang II vs. DKO + Ang II). **b** Ratio of heart weight to body weight in Ctrl and DKO mice treated with vehicle or Ang II; $n = 11$ (Ctrl + Vehicle), 19 (Ctrl + Ang II), 11 (DKO + Vehicle), and 19 (DKO + Ang II). $P < 0.0001$ (Ctrl + Vehicle

vs. Ctrl + Ang II), $P = 0.0006$ (DKO + Vehicle vs. DKO + Ang II). **c** Evaluation of mean BP levels in Ctrl and DKO mice using the radiotelemetry method at baseline and 7 days after Ang II administration; $n = 3$. The shaded area represents the dark phase (zeitgeber time (ZT) 12–24) for mice. **d** Expression levels of *Agt* mRNA in the skin of Ctrl and DKO mice treated with vehicle or Ang II; $n = 6$ (Ctrl + Vehicle), 11 (Ctrl + Ang II), 6 (DKO + Vehicle), and 11 (DKO + Ang II). **e** Immunoblot analysis of angiotensinogen protein in the skin of Ctrl and DKO mice treated with vehicle or Ang II; $n = 6$ (Ctrl + Vehicle), 11 (Ctrl + Ang II), 6 (DKO + Vehicle), and 11 (DKO + Ang II). Data were analyzed by two-way factorial analysis of variance (ANOVA) followed by Bonferroni's post-hoc test (**a**, **b**, **d** and **e**), or two-way repeated measures ANOVA with Bonferroni's post-hoc test (**c**), and are expressed as means ± standard deviation; *$P < 0.05$, **$P < 0.01$, and ***$P < 0.001$. Source data are provided as a Source Data file.

Plasma creatinine, urea nitrogen, and creatinine clearance at day 10 were also comparable between the genotypes (Supplementary Fig. 9b). Of note, tissue water and sodium contents in the skin and total body were comparable between the genotypes under Ang II administration (Table 2), suggesting that skin sodium accumulation was not an underlying mechanism for the exacerbated Ang II-induced hypertension in KO mice. To further validate these results, metabolic cage analysis was performed to evaluate the metabolic profiles of the mice over 10 consecutive days. This analysis showed that there were no significant between-genotype differences in the trends of body weight, water intake, food intake, urine volume, feces volume, urinary sodium excretion, and cumulative sodium balance, before and after Ang II administration (Fig. 5a, b). However, the water balance (calculated as water intake minus urine volume) was significantly reduced in Ang II-infused KO mice compared with Ang II-infused Ctrl mice (Fig. 5c), indicating that the urine volume per water intake was increased in Ang II-infused KO mice. Given the similar body weight changes and total body water contents between the genotypes after Ang II administration (Fig. 5a and Table 2), we suggest that the reduced water balance in Ang II-infused KO mice was mainly related to decreased extrarenal

water loss rather than exaggerated pressure diuresis caused by their hypertensive phenotype. This is further supported by the persistent significant difference in total balance, which includes water balance, food intake, fecal volume, and body weight changes, between the genotypes after Ang II administration. Consistent with these results and our hypothesis, TEWL was significantly decreased in Ang II-infused KO mice compared with that in Ang II-infused Ctrl mice (Fig. 5d), indicating that the decrease in extrarenal water loss in Ang II-infused KO mice was derived from decreased TEWL.

Skin vasoconstriction contributes to the exacerbation of Ang II-induced hypertension in mice lacking ATRAP in keratinocytes

TEWL represents passive cutaneous water loss, which is associated with blood flow in the skin[29,30]. Therefore, we hypothesized that the decrease in TEWL in Ang II-infused KO mice reflected an acceleration in skin vasoconstriction, which contributed to the exacerbation of Ang II-induced hypertension. To examine this hypothesis, we evaluated skin blood flow, TEWL, and BP under heat exposure. At a body temperature of 36.5 °C, measurements of TEWL and skin blood flow were significantly decreased, and BP was significantly increased in Ang II-

Table 2 | Analysis of sodium and water contents in the skin and total body of angiotensin II (Ang II)-infused control (Ctrl) and keratinocyte-specific ATRAP knockout (KO) mice

Variable	Ctrl + Ang II	KO + Ang II	*P*-value
No. of samples	11	12	
Skin wet weight (g)	3.34 ± 0.26	3.19 ± 0.29	0.2092
Skin dry weight (g)	1.49 ± 0.07	1.42 ± 0.11	0.0782
Skin sodium content (mmol)	0.227 ± 0.028	0.215 ± 0.024	0.2956
Skin sodium content (mmol/gDW)	0.152 ± 0.016	0.152 ± 0.019	0.9724
Skin water content (mL)	1.85 ± 0.21	1.77 ± 0.25	0.4319
Skin water content (mL/gDW)	1.24 ± 0.11	1.25 ± 0.19	0.8320
Total body wet weight (g)	17.16 ± 0.80	17.08 ± 0.85	0.8066
Total body dry weight (g)	6.35 ± 0.21	6.42 ± 0.37	0.5703
Total body sodium content (mmol)	1.022 ± 0.100	1.082 ± 0.084	0.1336
Total body sodium content (mmol/gDW)	0.161 ± 0.023	0.169 ± 0.017	0.2864
Total body water content (mL)	10.82 ± 0.70	10.66 ± 0.84	0.6294
Total body water content (mL/gDW)	1.71 ± 0.10	1.67 ± 0.17	0.5355

Data are expressed as means ± standard deviation and were analyzed using a two-sided unpaired *t* test; *$P < 0.05$, **$P < 0.01$, ***$P < 0.001$ vs. Ctrl. DW, dry weight.

infused mice compared with vehicle-treated mice, and this was observed in both genotypes (Fig. 5e). Notably, these changes between the treatment groups were greater in KO mice. However, these exaggerated differences in TEWL, skin blood flow, and BP between the genotypes treated with Ang II gradually disappeared as the body temperature increased (Fig. 5e), suggesting that skin vasoconstriction is responsible for the exaggerated BP elevation in Ang II-infused KO mice. To investigate the effects of skin tissue RAS on TEWL and skin blood flow in KO mice, we also measured these parameters in DKO mice. As shown in Supplementary Fig. 10, at a body temperature of 36.5 °C, the significant decreases in TEWL and skin blood flow, which were seen in Ang II-infused KO mice (Fig. 5d, e), were eliminated in Ang II-infused DKO mice. These findings suggest the substantial role of skin tissue RAS in the regulation of skin blood flow and TEWL.

Discussion

The pathogenesis of hypertension is inherently multifactorial and intricate, rendering its comprehension considerably challenging. Within this context, skin tissue has recently been implicated as a potential candidate for BP regulation[4–6]. The RAS, a well-established pathogenic factor of hypertension, has recently been reported to exist in the skin, where it plays roles in wound healing and skin fibrosis[13,14]. However, the physiological or pathophysiological mechanisms of the skin RAS in BP regulation remain unclear. Here, we approached these questions by performing human and animal experiments using human skin samples and mice lacking ATRAP specifically in keratinocytes. In human skin, we found that mRNA expression of *Agtrap*, an endogenous suppressor of AT1R signaling pathways, was significantly and negatively correlated with BP levels, whereas mRNA expression of *Agtr1*, a critical receptor for Ang II signal transduction, was not. In mice, we found that enhanced skin RAS activity resulting from ATRAP deletion in keratinocytes exacerbated Ang II-induced hypertension through skin vasoconstriction, which was eliminated by keratinocyte-specific AT1R deficiency or ARB treatment. Notably, despite recent reports implying the involvement of skin sodium accumulation in hypertension[7–9,31], we found that tissue water and sodium contents in the skin of mice were comparable between the *Agtrap*fl/fl Ctrl and K14Cre;*Agtrap*fl/fl KO genotypes. This result suggested that skin vasoconstriction, rather than skin sodium accumulation, was an underlying mechanism for the exacerbated Ang II-induced hypertension in this setting.

The largest organ in the body, the skin, contains a highly extensive vascular plexus featuring an abundance of pre-capillary arterioles with vascular smooth muscle cells[32]. These arterioles reportedly regulate skin blood flow and constitute the peripheral vascular resistance that regulates arterial BP[32]. Several previous studies have shown that alterations in skin microcirculation may affect arterial BP. Other groups demonstrated that hypoxia-inducible factor (HIF)−1α and HIF-2α in the skin differentially regulated arterial BP through modulating skin nitric oxide (NO) production in Ang II-infused mice[33], and whole-body ultraviolet A irradiation decreased BP in healthy human volunteers, along with increased NO release from the skin and skin vasodilation[34]. In addition, members of our group recently reported that skin and renal water loss in rodent models of psoriasis and renal injury drives compensatory skin vasoconstriction to suppress TEWL, subsequently leading to BP elevation[10,11]. In the current study, compared with Ang II-infused Ctrl mice, Ang II-infused KO mice exhibited significant decreases in skin blood flow and TEWL, along with an exaggeration of the Ang II-induced elevation in BP. These significant differences between the genotypes were mitigated by heat exposure, indicating a causality of skin vasoconstriction for the exacerbation in Ang II-induced hypertension in KO mice. We utilized the heating experiment to examine the possibility that skin vasoconstriction directly contributed to the arterial BP elevation[10]. Heat stress induces a redistribution of blood flow to peripheral tissues, leading to a substantial increase in skin blood perfusion. The enhancement of skin blood flow during heat stress is predominantly exerted via active vasodilation mediated by sympathetic cholinergic nerves, which provoke the release and activity of acetylcholine and other neurotransmitters[35]. Notably, it has also been reported that, under heat stress, splanchnic and renal blood flow are rather decreased, through vasoconstriction of vascular beds, to compensate for the increased blood flow in the skin and maintain BP[36]. Therefore, we conclude that the amelioration of exacerbated Ang II-induced hypertension by heat exposure in KO mice is mainly attributable to the attenuation of exaggerated skin vasoconstriction.

All RAS components necessary for Ang II synthesis, including angiotensinogen, renin, and ACE, are expressed in the skin. Indeed, a previous in vitro study indicated that keratinocytes have the ability to produce Ang II[13]. Furthermore, the presence of AT1R in the epidermis and dermal vascular endothelial cells suggests that the skin serves as both a source and a target of Ang II[13]. Thus, the skin might form the basis of local RAS activity independently of circulating RAS, similar to other tissues such as the brain, adipose tissue, and kidneys[37–39]. However, liver-derived angiotensinogen, the major source of circulating angiotensinogen, has been reported to strongly affect local angiotensinogen levels[40,41]. In the current study, keratinocyte-specific ATRAP deficiency caused Ang II-induced angiotensinogen excess specifically in the skin, which was consistently observed at the mRNA
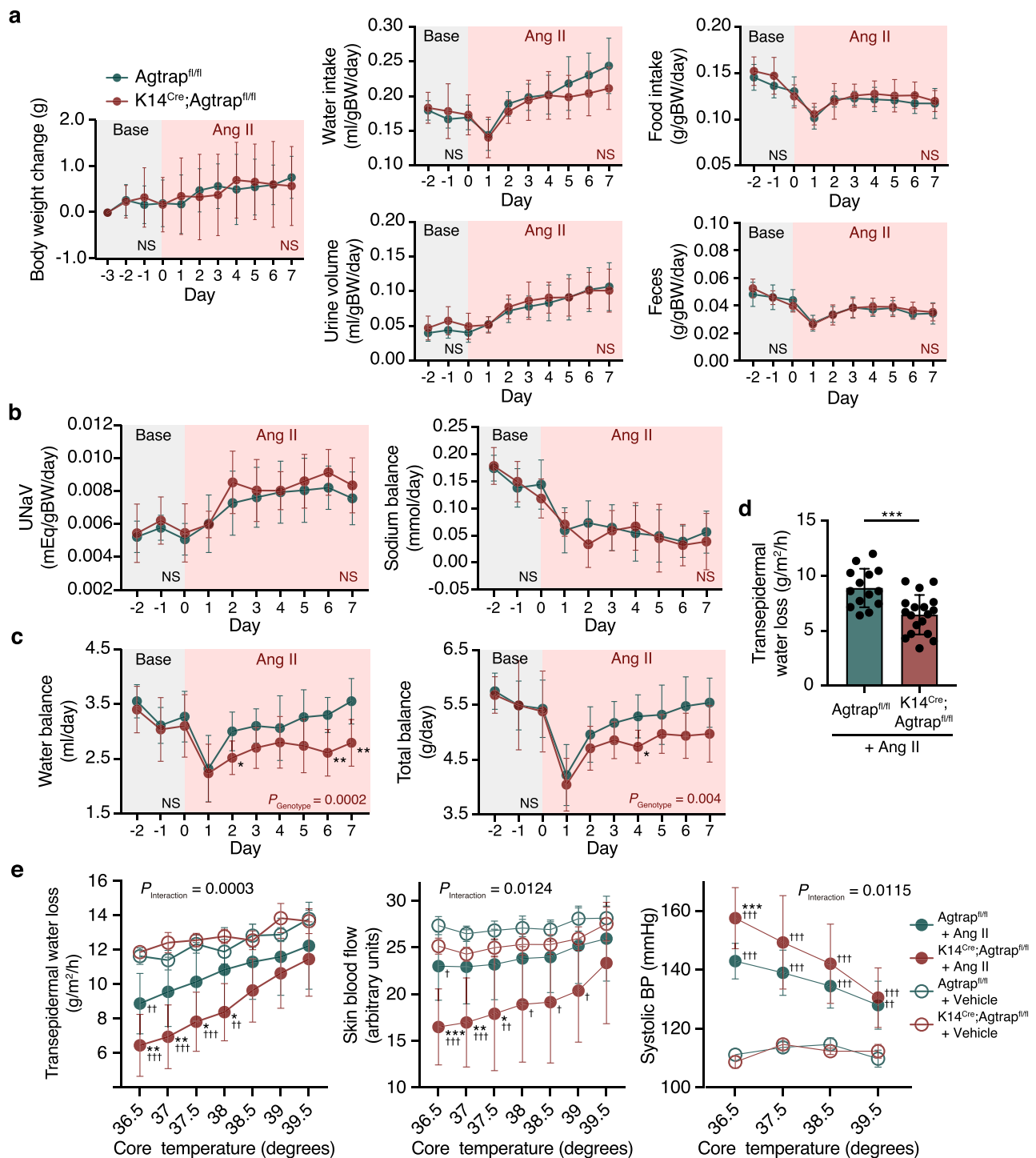
Fig. 5 | Keratinocyte-specific ATRAP deletion exacerbates angiotensin II-induced skin vasoconstriction. a, **b** Trends in body weight change, water intake, food intake, urine volume, feces volume, urinary sodium excretion, and cumulative sodium balance in control (Ctrl) and keratinocyte-specific ATRAP knockout (KO) mice before and after angiotensin II (Ang II) administration; $n = 10$ (Ctrl) and 11 (KO). **c** Calculation of water balance trends (volume of water intake − volume of urine) and total balance trends (water and food intake − body weight change and urine and fecal volume) in Ctrl and KO mice before and after Ang II administration; $n = 10$ (Ctrl) and 11 (KO). **d** Transepidermal water loss (TEWL) in Ang II-infused Ctrl and KO mice. $n = 14$ (Ctrl) and 18 (KO). $P = 0.0162$ (Ctrl + Ang II vs. DKO + Ang II). $P = 0.0006$ (Ctrl vs. KO). **e** Trends of TEWL, skin blood flow, and systolic blood pressure during the body heating experiment. The core temperature was gradually increased from

36.5 °C to 39.5 °C in Ctrl and KO mice treated with vehicle or Ang II. For TEWL and skin blood flow measurements: $n = 6$ (Ctrl + Vehicle), 14 (Ctrl + Ang II), 6 (KO + Vehicle), and 18 (KO + Ang II). For systolic blood pressure measurements: $n = 6$ (Ctrl + Vehicle), 17 (Ctrl + Ang II), 6 (KO + Vehicle), and 17 (DKO + Ang II). Exact Bonferroni's post-hoc P-values are provided as a Source Data file. Data were analyzed by two-way repeated measures analysis of variance with Bonferroni's post-hoc test (**a**–**c**, **e**), two-sided unpaired t test (**d**), and are expressed as means ± standard deviation. For Fig. 5e, exact Bonferroni's post-hoc P-values are provided in the Source Data file. *$P < 0.05$, **$P < 0.01$, and ***$P < 0.001$ vs Ang II-infused Ctrl group; †$P < 0.05$, ††$P < 0.01$, and †††$P < 0.001$ vs vehicle-infused group within the same genotype. Source data are provided as a Source Data file.
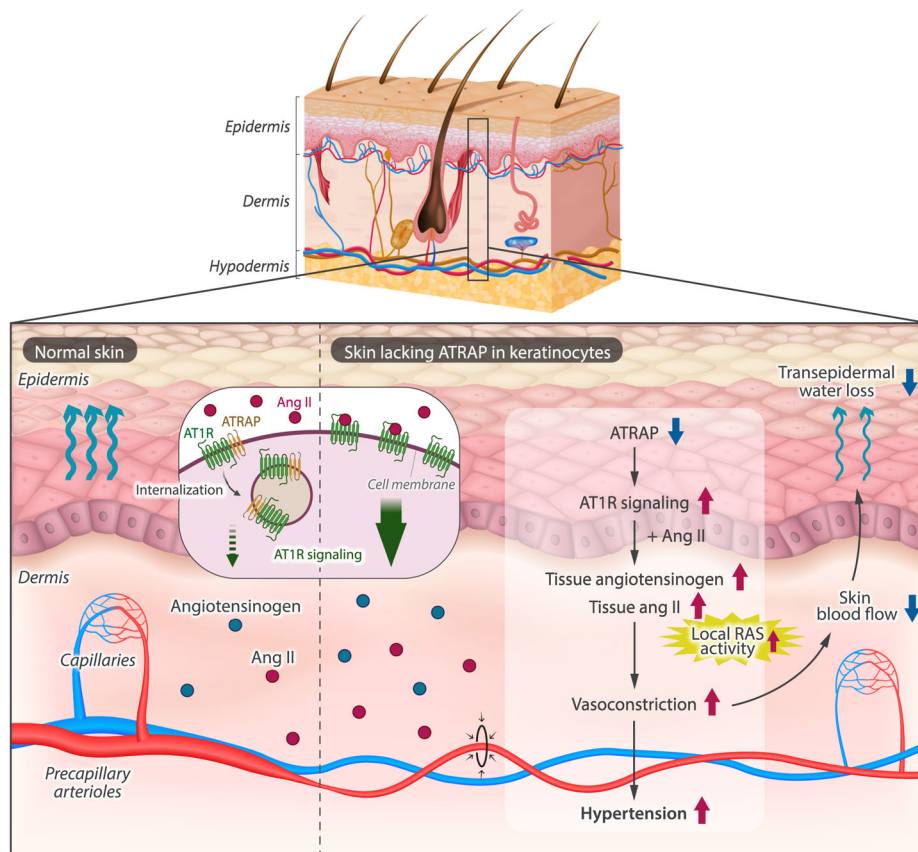
Fig. 6 | Schematic representation of the pathophysiological importance of the skin renin-angiotensin system (RAS) in angiotensin II (Ang II)-induced hypertension. Keratinocyte-specific Ang II type 1 receptor (AT1R)-associated protein (ATRAP) deficiency elicits downregulated AT1R internalization, which is associated with local RAS activation in the skin. In skin lacking ATRAP, Ang II-induced angiotensinogen production is accelerated through activating the Ang II-AT1R axis in keratinocytes, which may contribute to increased Ang II levels in the skin and exacerbated Ang II-induced hypertension through enhanced skin vasoconstriction. Figure partially created in BioRender. Taguchi, S. (2025) https://BioRender.com/c54c658.

and protein levels, suggesting Ang II-induced skin tissue RAS activation in KO mice. This is further supported by the fact that, although similar liver *Agt* mRNA expression and plasma Ang II levels were observed for both genotypes, Ang II levels in the skin were significantly increased in Ang II-infused KO mice. Interestingly, immunohistochemical analysis and western blotting analysis using epidermis samples suggested that keratinocytes are the main site of skin angiotensinogen excess in Ang II-infused KO mice. Furthermore, Ang II-induced angiotensinogen excess in skin lacking ATRAP was restored by additional keratinocyte-specific AT1R deficiency, suggesting that whole skin angiotensinogen excess in Ang II-infused KO mice was mainly mediated by the Ang II-AT1R axis in keratinocytes. These results support the concept of skin tissue RAS, which might involve a positive feedback loop for local RAS in the skin through the Ang II-AT1R axis. This is also suggested by previous studies demonstrating positive feedback between Ang II stimulation and local angiotensinogen production, especially in the kidneys[42–44]. The current study also revealed that KO mice exhibited enhanced Ang II-induced hypertension and skin vasoconstriction along with skin-specific angiotensinogen excess, all of which were abolished in DKO mice. Taken together, the results of this study suggest that keratinocyte-specific ATRAP deficiency accelerates Ang II-induced angiotensinogen production in the skin through activating the Ang II-AT1R axis in keratinocytes. This may contribute to increased Ang II levels in the skin, resulting in exacerbated Ang II-induced hypertension through enhanced skin vasoconstriction (Fig. 6).

This study has several limitations. First, although we consider skin vasoconstriction as a main factor affecting BP levels in our experimental model, blood flow in other organs was not evaluated in the body heating experiment, leaving it unclear to what extent the exacerbation of Ang II-induced hypertension in KO mice could be attributed to skin vasoconstriction. Second, because it was technically difficult measuring BP in anesthetized mice, TEWL/skin blood flow and BP were separately measured using different mice. Third, although this study revealed that skin RAS activity and vasoconstriction were partly involved in the pathogenesis of hypertension, the pathophysiological role of skin sodium accumulation remains unclear and should be further investigated in other hypertension models, such as the 5/6 nephrectomy and high salt-loading models. Fourth, because of the cross-sectional nature and limited sample size in the human experiments, the causal relationship between skin RAS activity and BP in humans is still unclear. This issue should be further investigated in prospective longitudinal studies with larger sample sizes.

In conclusion, the activation of the skin RAS contributes to arterial BP elevation through skin vasoconstriction. This insight underscores the recently posited involvement of the skin tissue in BP regulation while advancing our understanding of an alternative perspective of the RAS, one with an established pathogenic role in the development of hypertension. The skin RAS may have potential as a therapeutic target for the management of hypertension and should be further investigated.

Methods
Human experiments
The human experiments in this study were approved by the Human Studies Ethics Committee of Yokohama City University (IRB approval

no. B190500008), and all subjects provided written informed consent before enrollment, in compliance with the Declaration of Helsinki. Human skin tissue samples were obtained from consecutive 58 patients who underwent laparoscopic rectal cancer surgery with colostomy at Yokohama City University Hospital. Participants did not receive financial compensation for their involvement in this study. Samples were collected from men and women based on availability, irrespective of sex. Sex was determined by self-reporting. Immediately after the start of surgery, skin samples of approximately 15 mm in diameter were excised from the abdomen following a uniform method and procedure and using a metal scalpel. After removing sub-cutaneous adipose tissue, approximately 50 mg of each sample was trimmed and snap-frozen, and the remaining tissue was fixed in 4% paraformaldehyde in phosphate-buffered saline (PBS). Relevant clinical information and laboratory data were obtained from electronic medical records.

Office BP measurement

Office BP measurements were performed in accordance with the 2020 International Society of Hypertension Global Hypertension Practice Guidelines[45]. Briefly, BP measurements were taken in a quiet examination room at a comfortable temperature by well-trained physicians between 10:00 AM and 12:00 PM on the first day of hospitalization for the surgery. BP was measured on the left arm, three consecutive times at 1 min intervals, using a single validated electronic oscillometric upper-arm cuff device (UA-1020G, A&D, Japan). Before the measurement, patients were seated in a back-supported chair and allowed to relax for 3–5 min. Patients rested their arm on a table, with the mid-arm at heart level. Observers and patients were instructed not to speak during the measurements. The average of the last two measurements was taken as the office BP.

Animals

The animal experiments were performed following the National Institutes of Health Guidelines for the Use of Experimental Animals and were reviewed and approved by the Animal Studies Ethics Committee of Yokohama City University (IRB approval no. F-A-23-042). All experiments were performed in accordance with the ARRIVE guidelines. Mice bearing loxP-flanked *Agtrap* (*Agtrap*$^{fl/fl}$) and *Agtr1a* (*Agtr1a*$^{fl/fl}$) alleles were generated as described previously[46,47]. Keratinocyte-specific ATRAP-deficient mice (K14^{Cre};*Agtrap*$^{fl/fl}$, KO mice) were generated by crossing keratin 14 (K14)-Cre mice (purchased from the Jackson Laboratory; Stock No. 018964, USA) with *Agtrap*$^{fl/fl}$ mice. Keratinocyte-specific ATRAP/AT1R-deficient mice (K14^{Cre};*Agtrap*$^{fl/fl}$;*Agtr1a*$^{fl/fl}$, DKO mice) were generated by crossing KO mice with *Agtr1a*$^{fl/fl}$ mice. Littermate mice without Cre were used as controls (*Agtrap*$^{fl/fl}$ or *Agtrap*$^{fl/fl}$; *Agtr1a*$^{fl/fl}$, Ctrl mice). All mouse strains had a C57BL/6 genetic background and all experiments were conducted with male mice at 11–13 weeks of age to avoid the influence of the estrous cycle on physiological parameters. For all experiments, mice were randomly assigned to different experimental groups within the same genotype. To induce hypertension, mice were subcutaneously infused with Ang II at a concentration of 500 ng/kg/minute using osmotic minipumps (1007D, ALZET, USA). Mice were euthanized 7 days after Ang II administration, and plasma, abdominal skin, kidneys, and heart were harvested for subsequent analyses. Prior to skin tissue collection, hair was removed from the abdomen of each mouse using clippers and depilatory cream (Veet, Reckitt Benckiser, UK). To separate skin tissue into epidermis and dermis, skin tissue was incubated with 5 mg/mL Dispase II (Merck, Germany) diluted in Cnt-PR medium (CELLnTEC, Switzerland) for 6 h or overnight on ice. All experimental mice were housed in a controlled environment with a 12:12 light/dark cycle, ambient temperature (25 °C,) and humidity (55%), and free access to food and water. They were fed a standard diet with 0.5% NaCl, 3.6 kcal/g, and 13.3% energy as fat (Oriental MF, Oriental Yeast Co, Ltd., Japan).

ARB experiment

Olmesartan (20 mg/kg/day, O0510, Tokyo Chemical Industry, Japan), an AT1R blocker, was administered daily in drinking water from 2 days before Ang II administration (500 ng/kg/min) to the end of the experiment. BP was measured 3 days before and 6 days after Ang II administration using the tail-cuff method. Mice were euthanized 7 days after Ang II administration.

Body heating experiment

The body heating experiment was performed as previously described, with minor modifications[10,11]. Two days prior to the experiment, hair from each mouse was removed from the left and right dorsal lumbar regions, in the same area as probe heads used to obtain skin blood flow measurements (FLO-Lab and Type DS prove, Omegawave, Japan) and TEWL measurements (VAPO SCAN, AS-VT100RS, Asch Japan, Japan). During the heating experiment, the body temperature of each mouse was continuously monitored by a rectal probe. In TEWL and blood flow measurements, mice were anesthetized, and their body temperature was controlled by a heating lamp and a heating pad featuring a feedback system from the rectal probe (ThermoStar Homeothermic Monitoring System, RWD, USA). Body temperature was maintained at 36.5 °C before starting the experiment, and then gradually increased to 39.5 °C using the heating system. Skin blood flow and TEWL were measured at each 0.5 °C increase in body temperature. For BP measurements, mice in a conscious state were acclimatized to a restrainer for 10 minutes, during which time their rectal temperatures were monitored and adjusted to 36.5 °C by intermittently switching on the heating lamp. After the heating lamp was switched on continuously, the BP was measured repeatedly using the continuous measurement mode of the tail-cuff BP measurement system described below until the mouse reached a rectal temperature of 39.5 °C.

Tail-cuff BP measurement

Systolic BP and heart rate were measured via a noninvasive procedure using a computerized tail-cuff plethysmograph (MK-2000 BP monitor, Muromachi Kikai, Japan)[20,22]. Prior to the measurements, mice were acclimated in restrainers for 10 min. All measurements were performed in a blinded fashion by a well-trained investigator, between 10:00 and 14:00 to avoid diurnal BP variation. At least 10 measurements were taken for the analyses.

Radiotelemetry system

The 24 h BP measurements in conscious mice were performed using a radiotelemetry method[20,22]. Under anesthesia with isoflurane, an incision was made from the chin to the superior sternum, and the left common carotid artery was surgically exposed. A small incision was made in the artery adjacent to the bifurcation, and the tip of a BP transducer (PA-C10, Data Science International, USA) was placed in the artery. To avoid the influence of the surgery on circadian BP rhythm, the transmitter was implanted in the carotid artery 2 weeks before starting the Ang II administration. Measurements of 24-hour BP, heart rate, and activity were recorded at the baseline and 7 days after Ang II administration. Analyses were performed using Ponemah 6.3 (Data Science International).

Plasma volume measurement

Plasma volume in mice was measured using the Evans blue dye method[27,48]. Under general anesthesia with isoflurane, a catheter was placed in the left external jugular vein. Evans blue dye (50 μL of a 10 mg/mL solution; E2129, Sigma, USA) was injected through the catheter, followed by flushing with 200 μL sterile saline (0.9% NaCl) to confirm the completion of dye injection. Blood samples were taken from the heart 15 min after the injection, and plasma samples were obtained by centrifugation at 800 × *g*. Absorbance at 620 nm, which indicates Evans blue, was detected using a Biotek Synergy LX

Microplate Reader (Agilent Technologies, USA). The Evans blue concentration in plasma was calculated from a standard curve prepared by serial dilution of the dye, and the circulating plasma volume was calculated using a linear regression model.

Metabolic cage analysis

A metabolic cage analysis was performed, as described previously[26,49]. Mice were acclimated in the metabolic cage for 4 consecutive days. Then, consecutive daily measurements of metabolic parameters and 24 h urine collections were taken 3 days before and 7 days after Ang II administration to obtain data at the baseline and during Ang II administration. Mice were allowed free access to food and water during the metabolic cage analysis.

Total body and skin measurements of sodium and water

Water and sodium contents in the skin and carcass, which predominantly comprises muscle and bone, were measured by flame photometry of ash, as described previously with minor modifications[11,50]. Skin and carcass samples were desiccated for 72 h at 90 °C. Water content was calculated from the difference between wet and dry weights. The dried samples were ashed for 30 hours at 450 °C and then further ashed for 10 h at 600 °C. The skin and carcass ashes were dissolved in HNO_3. The sodium concentration of these samples was measured using a flame photometer (ANA-135, Tokyo Photoelectric Co. Ltd, Japan).

Biochemical assays

Blood samples were collected by cardiac puncture of mice that were euthanized in the fed state. Whole-blood samples were centrifuged at $800 \times g$ to separate plasma, which was snap-frozen and stored at −80 °C until use. Plasma creatinine, blood urea nitrogen, urinary sodium, and urinary creatinine were biochemically analyzed by Nagahama Life Science Laboratory (Oriental Yeast Co. Ltd.).

Ang II measurement

Ang II measurements were performed as described previously with modifications[11]. Frozen skin tissues were homogenized in ice-cold methanol. The homogenate was centrifuged at $800 \times g$ for 10 min, and the supernatant was evaporated overnight. Then, the evaporated skin samples were solubilized in angiotensin assay buffer consisting of 50 mmol/L sodium phosphate, 1 mmol/L ethylenediaminetetraacetate (EDTA), 0.25 mmol/L thimerosal, and 2.5 mg/mL of bovine serum albumin. Additionally, we collected blood samples into a tube including inhibitor cocktails consisting of 10 μL 500 mmol/L EDTA, 5 μL 4 mmol/L enalaprilat, 10 μL 125 mmol/L o-phenanthroline, and 1 mmol/L pepstatin in 95% ethanol. These were then centrifuged at $800 \times g$ for 20 min, and the supernatant was collected. Plasma and skin Ang II levels were measured by a combined method of solid phase extraction and enzyme-linked immunosorbent assay (ELISA)[51]. Plasma and skin samples were extracted on C18 reverse-phase bond elute columns, and ELISA was performed by a commercially available kit according to the manufacturer's protocols (Enzo Life Sciences, Inc., USA).

Real-time qRT-PCR analysis

Frozen human and mouse skin samples were pulverized using a Cryo-press (Microtech Nichion, Japan). Total RNA was extracted from human skin samples, as well as mouse skin, epidermis, dermis, kidney, heart, liver, and muscle tissues using RNeasy Universal Mini Kits (Qiagen, USA). The cDNA was synthesized using a SuperScript IV cDNA synthesis kit (Invitrogen, USA), in accordance with the manufacturer's protocol. Real-time qPCR analysis was performed by incubating the reverse transcription products with TaqMan Fast Advanced Master Mix and designed TaqMan probes (Applied Biosystems, USA) using a CFX96 Real-Time PCR System (Bio-Rad, USA). The TaqMan probes used for the PCR analysis were as follows: *Agtrap*, Hs01564425_m1 or Mm00507771_m1; *Agtr1*, Hs05043708_s1; *Agtr1a*, Mm01957722_s1; *Agt*,

Mm00599662_m1; *Ace*, Mm00802048_m1; *Ren1*, Mm02342887_mH; *Nppb*, Mm01255770_g1; *Acta1*, Mm00808218_g1; *Tnf*, Mm00443258_m1; *Il1b*, Mm00434228_m1; *Il6*, Mm00446190_m1; *Flg*, Mm00438930_m1; and *Tjp1*, Mm01320638_m1. The mRNA levels were normalized to those of *Gapdh* (Hs02786624_g1), *Actb* (Mm02619580_g1), or *Hprt* (Mm03024075_m1).

Histological and immunohistochemical analyses

Tissue samples were fixed overnight in 4% paraformaldehyde (in PBS) at 4 °C and then embedded in paraffin. Sections (4 μm thick) were stained with hematoxylin and eosin. Epidermal and dermal layer thicknesses were measured digitally at a minimum of 10 random points on each specimen using a fluorescence microscope (BZ-X800, Keyence, Japan). For immunohistochemical analyses, sections were incubated with anti-angiotensinogen antibody (1:150; #28101; Immuno-Biological Laboratories, Japan). All measurements were performed in a blinded manner.

Immunoblot analysis

Western blotting was performed, as described previously with modifications[52,53]. The epidermis was isolated by incubating the abdominal skin of mice in Dispase II, as described above. Frozen mouse skin samples were pulverized using a Cryo-press (Microtech Nichion, Japan). Samples were homogenized in sodium dodecyl sulfate (SDS)-containing sample buffer with cOmplete protease inhibitor cocktail (Roche, Switzerland) and phosphatase inhibitor (Pierce Phosphatase Inhibitor Mini Tablets, Thermo Fisher Scientific, USA), and were denatured by heating at 95 °C for 5 min. Protein concentrations were quantified using the bicinchoninic acid assay. Equal amounts of protein extracts were separated by 5–20% SDS-polyacrylamide gel electrophoresis and transferred to a polyvinylidene difluoride membrane. The membranes were blocked with 5% skim milk for 1 h at room temperature, and then trimmed and probed with a specific primary antibodies to angiotensinogen (1:4000; #79299, Cell Signaling Technology, USA) or GAPDH (1:3000; #5174, Cell Signaling Technology, USA). All antibodies used in this study were validated by the manufacturer. Horseradish peroxidase (HRP)-conjugated goat anti-rabbit immunoglobulin G secondary antibody (1:3000; #32460, Invitrogen, USA) was added for 1 h at room temperature. Immobilon Forte Western HRP substrate (Merck, USA) was used for detection. Images were captured using ChemiDoc Touch (Bio-Rad).

Statistical analysis

Statistical analyses were performed using Prism software version 9.5.0 (GraphPad Software, USA). The results are presented as means ± standard deviation. The Shapiro-Wilk test was used to assess normality. In the human experiments, relative mRNA expression levels of *Agtr1* and *Agtrap* were log-transformed because of their non-normal distribution, and Pearson's correlation analysis was used to evaluate the correlation between BP and gene expression levels. Statistical comparisons were made by two-way factorial analysis of variance (ANOVA) followed by Bonferroni's post-hoc test to compare differences between four groups, or the unpaired two-tailed Student's t test to compare differences between two groups. Two-way repeated measures ANOVA with Bonferroni's post-hoc test was used to test for differences over time. All statistical details of the experiments are provided in the figure legends. Statistical significance was defined as a two-sided P-value < 0.05. All statistical details, including the statistical tests used and exact n-values, are reported in the figure legends. Each data point represents a biological replicate and was obtained from either a single measurement or the average of multiple measurements.

Reporting summary

Further information on research design is available in the Nature Portfolio Reporting Summary linked to this article.

Data availability

Data supporting the findings of this study are available in the article and its Supplementary Information. Source data are provided as Source Data file and may be obtained from the corresponding authors upon request. Source data are provided in this paper.

References

1. Fuchs, F. D. & Whelton, P. K. High blood pressure and cardiovascular disease. *Hypertension* **75**, 285–292 (2020).
2. Worldwide trends in hypertension prevalence and progress in treatment and control from 1990 to 2019: a pooled analysis of 1201 population-representative studies with 104 million participants. *Lancet* **398**, 957–980 (2021).
3. Buhnerkempe, M. G. et al. Adverse health outcomes associated with refractory and treatment-resistant hypertension in the chronic renal insufficiency cohort. *Hypertension* **77**, 72–81 (2021).
4. Titze, J. & Luft, F. C. Speculations on salt and the genesis of arterial hypertension. *Kidney Int.* **91**, 1324–1335 (2017).
5. Minegishi, S., Luft, F. C., Titze, J. & Kitada, K. Sodium handling and interaction in numerous organs. *Am. J. Hypertens.* **33**, 687–694 (2020).
6. Kitada, K. & Nishiyama, A. Revisiting blood pressure and body fluid status. *Clin. Sci.* **137**, 755–767 (2023).
7. Kopp, C. et al. 23Na magnetic resonance imaging-determined tissue sodium in healthy subjects and hypertensive patients. *Hypertension* **61**, 635–640 (2013).
8. Schneider, M. P. et al. Skin sodium concentration correlates with left ventricular hypertrophy in CKD. *J. Am. Soc. Nephrol.* **28**, 1867–1876 (2017).
9. Nikpey, E. et al. High-salt diet causes osmotic gradients and hyperosmolality in skin without affecting interstitial fluid and lymph. *Hypertension* **69**, 660–668 (2017).
10. Wild, J. et al. Aestivation motifs explain hypertension and muscle mass loss in mice with psoriatic skin barrier defect. *Acta Physiol.* **232**, e13628 (2021).
11. Kovarik, J. J. et al. Adaptive physiological water conservation explains hypertension and muscle catabolism in experimental chronic renal failure. *Acta Physiol.* **232**, e13629 (2021).
12. Ogura, T. et al. Contributions of renal water loss and skin water conservation to blood pressure elevation in spontaneously hypertensive rats. *Hypertens. Res.* **46**, 32–39 (2023).
13. Steckelings, U. M. et al. Human skin: source of and target organ for angiotensin II. *Exp. Dermatol.* **13**, 148–154 (2004).
14. Silva, I. M. S. et al. The role of the renin-angiotensin system in skin physiology and pathophysiology. *Exp. Dermatol.* **29**, 891–901 (2020).
15. Azushima, K., Morisawa, N., Tamura, K. & Nishiyama, A. Recent research advances in renin-Angiotensin-aldosterone system receptors. *Curr. Hypertens. Rep.* **22**, 22 (2020).
16. de Gasparo, M., Catt, K. J., Inagami, T., Wright, J. W. & Unger, T. International union of pharmacology. XXIII. The angiotensin II receptors. *Pharmacol. Rev.* **52**, 415–472 (2000).
17. Forrester, S. J. et al. Angiotensin II signal transduction: An update on mechanisms of physiology and pathophysiology. *Physiol. Rev* **98**, 1627–1738 (2018).
18. Wakui, H. The pathophysiological role of angiotensin receptor-binding protein in hypertension and kidney diseases: Oshima Award Address 2019. *Clin. Exp. Nephrol.* **24**, 289–294 (2020).
19. Tamura, K., Azushima, K., Kinguchi, S., Wakui, H. & Yamaji, T. ATRAP, a receptor-interacting modulator of kidney physiology, as a novel player in blood pressure and beyond. *Hypertens. Res.* **45**, 32–39 (2022).
20. Wakui, H. et al. Cardiac-specific activation of angiotensin II type 1 receptor-associated protein completely suppresses cardiac hypertrophy in chronic angiotensin II-infused mice. *Hypertension* **55**, 1157–1164 (2010).
21. Wakui, H. et al. Intrarenal suppression of angiotensin II type 1 receptor binding molecule in angiotensin II-infused mice. *Am. J. Physiol. Renal. Physiol.* **299**, F991–F1003 (2010).
22. Wakui, H. et al. Activation of angiotensin II type 1 receptor-associated protein exerts an inhibitory effect on vascular hypertrophy and oxidative stress in angiotensin II-mediated hypertension. *Cardiovasc. Res.* **100**, 511–519 (2013).
23. Wakui, H. et al. Renal tubule angiotensin II type 1 receptor-associated protein promotes natriuresis and inhibits salt-sensitive blood pressure elevation. *J. Am. Heart Assoc.* **4**, e001594 (2015).
24. Azushima, K. et al. Adipocyte-specific enhancement of angiotensin II type 1 receptor-associated protein ameliorates diet-induced visceral obesity and insulin resistance. *J. Am. Heart Assoc.* **6**, e004488 (2017).
25. Ohki, K. et al. Angiotensin II type 1 receptor-associated protein inhibits angiotensin II-induced insulin resistance with suppression of oxidative stress in skeletal muscle tissue. *Sci. Rep.* **8**, 2846 (2018).
26. Ohsawa, M. et al. Deletion of the angiotensin II type 1 receptor-associated protein enhances renal sodium reabsorption and exacerbates angiotensin II-mediated hypertension. *Kidney Int.* **86**, 570–581 (2014).
27. Kobayashi, R. et al. An angiotensin II type 1 receptor binding molecule has a critical role in hypertension in a chronic kidney disease model. *Kidney Int.* **91**, 1115–1125 (2017).
28. Haruhara, K. et al. Deficiency of the kidney tubular angiotensin II type1 receptor-associated protein ATRAP exacerbates streptozotocin-induced diabetic glomerular injury via reducing protective macrophage polarization. *Kidney Int.* **101**, 912–928 (2022).
29. Rodrigues, L. M., Pinto, P. C., Magro, J. M., Fernandes, M. & Alves, J. Exploring the influence of skin perfusion on transepidermal water loss. *Skin Res. Technol.* **10**, 257–262 (2004).
30. Nomura, T. et al. Relationships between transepidermal water loss, cutaneous microcirculatory function and autonomic nervous activity. *Int. J. Cosmet. Sci.* **39**, 275–283 (2017).
31. Kopp, C. et al. (23)Na magnetic resonance imaging of tissue sodium. *Hypertension* **59**, 167–172 (2011).
32. Cracowski, J. L. & Roustit, M. Human skin microcirculation. *Compr. Physiol.* **10**, 1105–1154 (2020).
33. Cowburn, A. S. et al. HIF isoforms in the skin differentially regulate systemic arterial pressure. *Proc. Natl. Acad. Sci. USA* **110**, 17570–17575 (2013).
34. Liu, D. et al. UVA irradiation of human skin vasodilates arterial vasculature and lowers blood pressure independently of nitric oxide synthase. *J. Invest. Dermatol.* **134**, 1839–1846 (2014).
35. Kellogg, D. L. Jr. In vivo mechanisms of cutaneous vasodilation and vasoconstriction in humans during thermoregulatory challenges. *J. Appl. Physiol.* **100**, 1709–1718 (2006).
36. Cheng, J. L. & MacDonald, M. J. Effect of heat stress on vascular outcomes in humans. *J. Appl. Physiol.* **126**, 771–781 (2019).
37. Crowley, S. D., Navar, L. G., Prieto, M. C., Gurley, S. B. & Coffman, T. M. Kidney renin-angiotensin system: Lost in a RAS cascade. *Hypertension* **81**, 682–686 (2024).
38. Lin, H. et al. Kidney Angiotensin in cardiovascular disease: Formation and drug targeting. *Pharmacol. Rev.* **74**, 462–505 (2022).
39. Kobori, H., Nangaku, M., Navar, L. G. & Nishiyama, A. The intrarenal renin-angiotensin system: from physiology to the pathobiology of hypertension and kidney disease. *Pharmacol. Rev.* **59**, 251–287 (2007).
40. Matsusaka, T. et al. Liver angiotensinogen is the primary source of renal angiotensin II. *J. Am. Soc. Nephrol.* **23**, 1181–1189 (2012).
41. Jang, H. S. et al. Hepatic and proximal tubule angiotensinogen play distinct roles in kidney dysfunction, glomerular and tubular injury, and fibrosis progression. *Am. J. Physiol. Renal. Physiol.* **323**, F435–f446 (2022).
42. Ingelfinger, J. R. et al. Rat proximal tubule cell line transformed with origin-defective SV40 DNA: autocrine ANG II feedback. *Am. J. Physiol.* **276**, F218–F227 (1999).

43. Kobori, H., Harrison-Bernard, L. M. & Navar, L. G. Enhancement of angiotensinogen expression in angiotensin II-dependent hypertension. *Hypertension* **37**, 1329–1335 (2001).

44. Kobori, H., Harrison-Bernard, L. M. & Navar, L. G. Expression of angiotensinogen mRNA and protein in angiotensin II-dependent hypertension. *J. Am. Soc. Nephrol.* **12**, 431–439 (2001).

45. Unger, T. et al. 2020 International society of hypertension global hypertension practice guidelines. *Hypertension* **75**, 1334–1357 (2020).

46. Ohki, K. et al. ATRAP Expression in brown adipose tissue does not influence the development of diet-iduced metabolic disorders in mice. *Int. J. Mol. Sci.* **18**, 676 (2017).

47. Matsusaka, T. et al. Angiotensin receptor blocker protection against podocyte-induced sclerosis is podocyte angiotensin II type 1 receptor-independent. *Hypertension* **55**, 967–973 (2010).

48. Cole, J. M. et al. Mice lacking endothelial ACE: normal blood pressure with elevated angiotensin II. *Hypertension* **41**, 313–321 (2003).

49. Wakui, H. et al. Enhanced angiotensin receptor-associated protein in renal tubule suppresses angiotensin-dependent hypertension. *Hypertension* **61**, 1203–1210 (2013).

50. Titze, J. et al. Reduced osmotically inactive Na storage capacity and hypertension in the Dahl model. *Am. J. Physiol. Renal. Physiol.* **283**, F134–F141 (2002).

51. Kobori, H., Nishiyama, A., Harrison-Bernard, L. M. & Navar, L. G. Urinary angiotensinogen as an indicator of intrarenal Angiotensin status in hypertension. *Hypertension* **41**, 42–49 (2003).

52. Maeda, A. et al. Angiotensin receptor-binding protein ATRAP/Agtrap inhibits metabolic dysfunction with visceral obesity. *J. Am. Heart Assoc.* **2**, e000312 (2013).

53. Taguchi, S. et al. Effects of tumor necrosis factor-α inhibition on kidney fibrosis and inflammation in a mouse model of aristolochic acid nephropathy. *Sci. Rep.* **11**, 23587 (2021).

Acknowledgements

Author contributions

S.T. designed and conducted experiments, analyzed and interpreted data, and wrote the manuscript. K.A. conceptualized and designed the study, conducted experiments, analyzed and interpreted data, wrote the manuscript, and was responsible for project administration. K.K. designed experiments, conducted experiments including ashing-flame photometry and biochemical assays, analyzed and interpreted data, and reviewed and edited the manuscript. N.M analyzed and interpreted data and reviewed and edited the manuscript. T.M. designed and conducted experiments using *Agtr1a*^fl/fl^ mice and reviewed and edited the manuscript. K.N., A.I., I.E., K.K., Y.R., and A.S. provided human resources. S. Kidoguchi, R.M., S. Kinguchi, R.K., A.Y., H.W., A.N., and K.T. reviewed and edited the manuscript. H.W., A.N., and K.T. supervised the study.

Competing interests

The authors declare no competing interests.

Additional information

¹Department of Medical Science and Cardiorenal Medicine, Yokohama City University Graduate School of Medicine, Yokohama, Japan. ²Department of Pharmacology, Faculty of Medicine, Kagawa University, Kagawa, Japan. ³Programme in Cardiovascular and Metabolic Disorders, Duke-NUS Medical School, Singapore, Singapore. ⁴Division of Nephrology and Hypertension, Department of Internal Medicine, The Jikei University School of Medicine, Tokyo, Japan. ⁵Department of Gastroenterological Surgery, Yokohama City University Graduate School of Medicine, Yokohama, Japan. ⁶Department of Surgery, Yokohama City University, Yokohama, Japan. ⁷Department of Basic Medicine, Tokai University School of Medicine, Isehara, Japan. ⁸Department of Investigative Medicine, Graduate School of Medicine, University of the Ryukyus, Okinawa, Japan. ⁹Yokohama City University Medical Center, Yokohama, Japan. ✉e-mail: azushima@yokohama-cu.ac.jp; hiro1234@yokohama-cu.ac.jp